



A robust model for improving the quality of underwater images using enhancement techniques

Nishant Singh¹ · Aruna Bhat²

Received: 1 April 2022 / Revised: 24 March 2023 / Accepted: 22 April 2023 /
Published online: 12 May 2023

© The Author(s), under exclusive licence to Springer Science+Business Media, LLC, part of Springer Nature 2023

Abstract

Underwater image enhancement is an important research field that is now being addressed across the world. The primary reason for this is that water scatters and absorbs light, resulting in images with extremely low contrast and color cast. Hence, in order to overcome this issue with underwater images, we designed a simple and effective method. This method is split into two parts. The first section focuses on boosting contrast, while the second on improving color. To begin with, under the RGB colour model, contrast enhancement equalizes the G and B channels. Each R, G, and B channel's histogram is then redistributed using effective parameters connected with the intensity distribution in the input image and the wavelength attenuation of various colors underwater. The noise is subsequently reduced using a bilateral filtering technique, which only keeps important facts in an underwater image but also increases local information. In the second section, the color is enhanced by increasing the L component and modifying the 'a' and 'b' components of the CIE lab color space. Experiment findings show that the suggested method outperforms alternative strategies. Our enhanced results stand out for their brilliant color, greater contrast, and enhanced features. When compared to other approaches, the values of entropy, mean square error (MSE), peak signal to noise ratio (PSNR), underwater color image quality evaluation (UCIQE), and underwater image quality measures are 7.88, 920.20, 18.92, 0.596, and 2.734, respectively. This technique improves image quality by increasing entropy, PSNR, and UCIQE values while lowering MSE. It is an entirely algorithm-based technique that is independent by image datasets. The images used to evaluate the results come from a variety of datasets, and their enhanced performance confirms their robustness. Because of its single image-based approach, our method is very compelling in terms of processing speed. Comprehensive findings on a variety of underwater image datasets demonstrate that our approach outperforms the vast majority of them. For these reasons, the Comparative Universal Stretching approach is better than others.

Keywords Underwater image enhancement · Contrast Improvement · Color Improvement · Comparative Universal Stretching (CUS)

✉ Aruna Bhat
aruna.bhat@dtu.ac.in

Extended author information available on the last page of the article

1 Introduction

Underwater image enhancement for clear images and real videos is very important for applications like underwater robots, marine ecology, underwater biological recognition, underwater archaeology and many more [34]. However, with respect to images in the natural environment, the images are visible very poor and more complex in the ocean. There are primarily two reasons for this: the first is light absorption, reflection, and scattering; the second is the underwater atmosphere, including the existence of noise and water turbidity. If we assume crystal clear water with a very high attenuation lever, even though the beam of light is absorbed and scattered. When the light is travelling to the camera, the beam of light is deviated and reflected many number of times by the particles that are present in underwater [1]. One basic property of water is that the higher the wavelength of light, the quicker the light disappears. Due to this property, in comparison to green and blue, red light is more affected. Hence the images are appeared blue tone in underwater [7].

Underwater images get affected by poor visibility of light which significantly fades while travelling in the water, thus impacting the result in terms of haziness and poor contrast. The visibility of light gets affected under water by the distance travelled i.e., around twenty meter in case of clear water and approximately five meters or less in case of cloudy water. Scattering and absorption affects the travelling of light in water. In scattering the direction of light path is changed while in absorption light energy is reduced. Hence scattering and absorption influence overall performance of underwater imaging system.

Underwater image restoration and enhancement algorithms are two types of underwater image clarity approaches. The aim of underwater image restoration techniques is to discover a way to reverse the physical degradation process and repair the deteriorated underwater image to a cleaner underwater image. Underwater image enhancement algorithms, which are based on current image enhancement techniques, either emphasize the region of interest or minimize the non region of interest by altering the pixels of the actual image to increase the clarity of underwater images. It is due to the fact that they do not take into account the underwater optical imaging method, enhancement methods are simple and effective.

In general, underwater image enhancement and restoration are mainly done by two types of techniques: one is based on the physical based method used by the restoration technique and second is based on the image based method used by the enhancement technique [8, 27]. The physical based method improves underwater images by taking into account the basic physics of light transmission through the water. Zhao et al. enhance underwater images by obtaining the natural optical attribute of water, from the background color of the image [12]. Haziness occurs in images due to the scattering and absorption of light inside water, as well as color cast, and a very similar process occurs in a normal environment due to foggiess. Dark Channel Prior (DCP) [9] is one of the core dehazing methods that have been commonly used in the improvement of underwater images [10, 11]. The Wavelength compensation and image dehazing (WCID) [3] algorithm not only compensates for the attenuation divergence along with the transmission path but also controls the feasible occurrence of artificial light. It retains the color cast while also increasing the clarity of underwater images. WCID has some drawbacks also, like it needs high computing resources and too much computing time.

In comparison to physical based methods, image based methods are more efficient and also simpler because we have to focus on the image instead of the capturing mechanism [24]. Color equalization techniques are commonly employed to address the color casting issue in underwater images. In which the blue and green color is highly dominant due to their wavelength property in the water medium. For this reason, the

underwater images are generally blue toned in nature. Iqbal et al. developed an unsupervised color improvement method (UCM) [25], also offered an integrated color model (ICM) [23]. These methods not only increase the color cast, but also the contrast of underwater images. It used RGB color mode histogram stretching and then HSI color model saturation-intensity stretching. UCM is different from ICM as they modify both green and red channels depending on the hypothesis of Von Kries. It stretches either one or both sides, depending on the characteristics of the RGB channel. Whereas in the output of these two models, there is no such fruitful difference, even though there is still blue and green illumination present [21]. Due to this, there is some noise in the enhanced images. However, instead of considering the peculiarities of distinct channels, the Rayleigh distribution is used to stretch each one [35].

Considering the numerous advantages of the mentioned enhancement techniques, there are certain limitations in underwater image color correction. These techniques in [30] conduct the piece wise stretching process for color correction, without paying attention to the attenuation adjustment of underwater images. The author in [13], first converts the color channel of every input image into lower, middle, and upper color channels based on the total pixel intensity of each color channel, and then designs dedicated fractions to compensate for the loss of the middle and lower color channels due to light attenuation at different wavelengths. As a result, in the underwater imaging environment, we adaptively split every color channel into a foreground image and a background image based on the fact that the region nearer the source of light is brighter than the region distant from the light source. The background-stretched and foreground-stretched images for each color channel are incorporated depending on the best possible threshold point to enhance the contrast of the output image. But the enhancement achieved by using these techniques is not that accurate.

Unlike these algorithms, we thus suggest a novel approach, namely comparative universal stretching (CUS) based on contrast and color improvement. The contrast improvement is mainly based on the GB channel equalization and stretching of the histogram in RGB color space. It calculates the tensile range factor using original image distribution features as well as light absorption of different wavelengths in water. Once the image is extended in RGB color space, the bilateral filter is used, which is a non iterative and simple method. This bilateral filter is used to efficiently confine the fine details of an image by smoothing the edges. After performing contrast improvement on the original image, we have to perform color improvement on the resultant image. The resultant image is the output of the contrast improvement method. This approach preserves image details while also increasing visibility. The importance of this model with respect to ICM, DCP and UCM models is represented by having the highest entropy [4], PSNR and UCIQE [36] and a lower value in Q-MOS [15] and MSE [16]. As, it is a single image based system [20], it is independent from the datasets, which provide the robustness of the system. To justify their robustness, we applied our model to eight different datasets and evaluated the images. On the basis of result evaluation, we can easily conclude that the images enhanced using our comparative universal stretching method in the UIEB, RUIE, EUVP, UFO-120, and U45 datasets are above average, while those in the LSUI, Underwater MOT, and DUO datasets are below average. The detailed explanation is given in Sect. 4.

In Sect. 2 we briefly discuss the correlated processing work, which has been used to enhance the images, and in Sect. 3 we elaborate in detailed on the proposed work. Section 4 contains the evaluation of the results. In last, give the conclusion in Sect. 5.

2 Related work

2.1 Underwater model

Various well-defined image hazing models [29, 31] are generally used to estimate the transmission equation of the scattered background light in an underwater scene. The equation is given below:

$$I_{\lambda}(x) = J_{\lambda}(x)t_{\lambda}(x) + (1 - t_{\lambda}(x))B_{\lambda} \quad (1)$$

where λ is the light wavelength that belongs to red, green and blue. x is the underwater image $I_{\lambda}(x)$ pixel point. $J_{\lambda}(x)$ denotes the light at sight location x . $t_{\lambda}(x)$ denotes the residual energy ratio (RER). RER is the ratio of reflection in underwater from location x to back to camera. Uniform background light is represented by B_{λ} . $J_{\lambda}(x)t_{\lambda}(x)$ represents the straight attenuation of scene radiant $J_{\lambda}(x)$ in underwater [28]. The RER $t_{\lambda}(x)$ is depends upon the λ as well as the site camera distanced(x), which shows the overall effects of color change which has been suffered by the wavelength of light in underwater distance $d(x)$ and light scattering. Therefore $t_{\lambda}(x)$ can be defined as:

$$t_{\lambda}(x) = NRER(\lambda)^{d(x)} \quad (2)$$

where NRER is normalized RER, which defines the proportion of residual energy ratio to original energy for a minimum single unit of distance transmitted. As we know, the green & blue light have a higher frequency because of their shorter wavelengths, and therefore they attenuate extremely lower as a comparison to the red light. For this reason, as we move deep inside the sea, the images appear as blue toned images. The values of the light wavelength of NRER (λ) are defined as follows:

$$NRER(\lambda) = \begin{cases} 0.83 \sim 0.90 & \text{if } \lambda = 590 \sim 750 \mu\text{m (Red)} \\ 0.90 \sim 0.95 & \text{if } \lambda = 490 \sim 590 \mu\text{m (Green)} \\ 0.95 \sim 0.99 & \text{if } \lambda = 400 \sim 490 \mu\text{m (Blue)} \end{cases} \quad (3)$$

We are using these values to predict the range of RGB channels in the CUS model.

2.2 Histogram stretching

The underwater images have very low visibility and contrast because of the very low range of histograms and relatively concentrated distribution. To overcome this problem, we use histogram stretching, which gives us a fair distribution of pixels in the image channels across the dynamic range. This improves the visibility and contrast in the image. Contrast stretching function is given as in Eq. (4). [21, 23][17, 18]

$$p_o = (p_i - a) + \frac{c - d}{b - a} + d \quad (4)$$

where p_i is the intensity value of the input pixel, p_o is the intensity value of the output pixel. The min & max intensity values of the actual image and the desired output image is represented by a, b & c, d , respectively. c & d are constant in a global stretching and are frequently fixed to 255 & 0 respectively; a & b are chosen at 0.2% & 99.8% in the original image's entire histogram.

3 Proposed work

Generally our suggested model is consists of three basic steps: contrast improvement, color improvement, and quality evaluation as shown in Fig. 1.

In contrast improvement, first of all, we are doing RGB channel decomposition. After that, we perform color equalization on green and blue channels. Then we determine the adaptive stretching range. After that, we perform comparative universal stretching on the image. Finally, while keeping the information of the needed colorful underwater image, we use a bilateral filter to eliminate the noise created by the aforesaid transformation [28]. This will not only diminish the color cast result because of the light absorption and scattering, but also reduce the effect of the low contrast. Once we performed all the steps in contrast improvement, we got the resultant image. After that, we performed color improvement on the resultant image [37]. In color improvement, first of all, we change the image into CIELAB color model. We extend L parameter of the image using basic global histogram stretching and correct the a & b parameters in CIE Lab color model. The adaptive stretching of L, a, b improves the image's brightness and saturation, resulting in a more vibrant color. After performing contrast improvement and color improvement, to estimate the quality of our designed model, we use a few quality evaluation parameters. Now we are going to elaborate in detail on contrast improvement and color improvement.

3.1 Contrast improvement

Figure 2 shows the sequence used in contrast improvement.

3.1.1 Color equalization on GB channel

Images are rarely color balanced appropriately when taken underwater. We begin color equalization for the underwater image after RGB channel decomposition. According to Von Kries hypothesis [25, 23] modified color values in RGB components, keeping the leading

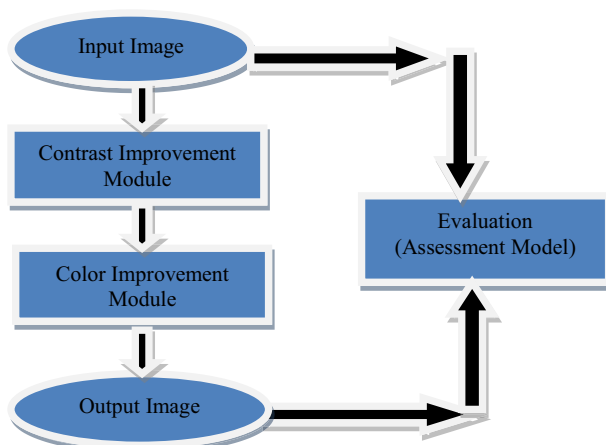


Fig. 1 Comparative Universal Stretching (CUS) Model

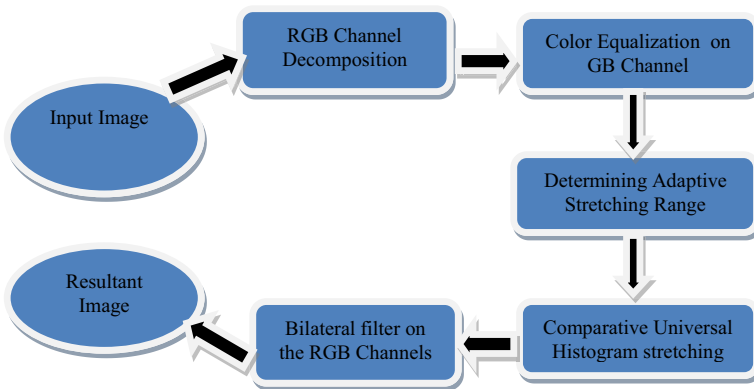


Fig. 2 Sequence used in contrast improvement

color cast channel constant. As per UCM model, if one channel's average is very low, the channel must increase with a larger multiplier, resulting in incorrect image color processing. Whereas motivated by the Gray World Assumption Theory (GWAT)[2], in a perfect image, the mean value of any color object is always gray. Hence, we improve the green and blue channels with the help of the following assumptions,

$$(R_{avg} + G_{avg} + B_{avg})/3 = 0.5 \quad (5)$$

where R_{avg} , G_{avg} , B_{avg} and are the normalized mean values of the recovered RGB channels. and are the normalized mean values of the recovered RGB channels.

$$\begin{aligned} R_{avg} &= \frac{1}{255 * MN} \sum_{i=1}^M \sum_{j=1}^N I_g(i, j), \theta_g = \frac{0.5}{G_{avg}} \\ B_{avg} &= \frac{1}{255 * MN} \sum_{i=1}^M \sum_{j=1}^N I_b(i, j), \theta_b = \frac{0.5}{B_{avg}} \end{aligned} \quad (6)$$

Pixel values can vary between 0 and 256. Every value denotes a color code. The calculation on these large numerical values may get more difficult when processing the image as it is, i.e., by taking the simple mean value. It can be minimized by normalizing the numbers to the range between 0 to 1. As a result, the numbers would be minimal and the calculation would be easy as well as quicker. Pixel values vary between 0 to 256; apart from 0, the range is 255. Hence, dividing all the numbers by 255 (i.e., the standard deviation), will convert them to a range of 0 to 1. That is the reason for taking the normalized mean value instead of the simple mean value in Eq.(6).

With the help of GWAT, we improve the G & B channel. The R channel is not taken into attention here since the red light in water is difficult to correct with basic color equalization. If we consider the red light, then it brings red over saturation. The above equation is defined for computing channels color equalization coefficient i.e. θ_g & θ_b , respectively. The underwater image size is given by $M * N$. Depends upon the color equalization coefficients θ_g & θ_b , the intensity of the G channel and B channel is modified by changing θ_g and θ_b respectively. After this, we now have to perform comparative universal stretching for image channels.

3.1.2 Comparative universal stretching (CUS)

The overall histogram stretching method typically employs the same values for each R, G, B channel of an image, neglecting the histogram allocation features of individual channels and images. If predefined values for example (0, 255) have been used in (4), some color channels either over or under stretched, causing destruction to the input image's features. Due to the transmission principle of light in underwater, to repair the distorted images, we must use the contrast improvement approach. Based on the following observation in underwater images, the RGB channel's histogram distribution requirements are as follows: The histogram of red light in most underwater images is decided in the band [50, 150], whereas in G & B channel have values in [70, 210]. Due to this the histogram stretching is sensitive to channels. We rewrite the comparative universal stretching in Eq. (7) to distinguish it with global histogram stretching in Eq. (4).

$$p_{out} = (p_{in} - I_{min}) \left(\frac{O_{max} - O_{min}}{I_{max} - I_{min}} \right) + O_{min} \quad (7)$$

where p_{in} is the input pixel, p_{out} is the output pixel. I_{min} and I_{max} are the adaptive parameters before the stretching images. O_{min} and O_{max} are the adaptive parameters after the stretching images. After this, we'll go through how to calculate the stretching range (I_{min}, I_{max}) and the desired range (O_{min}, O_{max}).

3.1.3 Determining adaptive stretching range

If we consider the histogram distribution of different underwater images, it is seen that, histogram distribution in RGB channel is comparable to variant of the Rayleigh distribution described as (8), and that is an ongoing probability proportion for positive valued random variables.

$$RayleighDistribution = \frac{x}{a^2} e^{-x^2/2a^2}, x \geq 0, a > 0 \quad (8)$$

In Eq. (8), the distribution's scaling parameter a is the mode, which is the highest in $R, G \& B$ channel histogram. It is worth noting that, when a channel's allocation follows a regular pattern, its midpoint and mode are almost identical. In the histogram stretching, we use the mode result as a borderline to determine the minimum intensity level as the left and maximum intensity level as the right of the original image.

Because underwater images are impacted by a variety of causes, stretching ranges between 0.1% and 99.9% of the histogram are commonly used to decrease the impact of certain high pixels in comparative universal stretching. If the histogram is not regularly distributed, the procedure of removing the same quantity of pixels from both ends in histogram is not appropriate. To compute the I_{min} and I_{max} for each RGB channel, we partition the top and the bottom portion of the intensity values, as shown in Eq. (9).

$$\begin{aligned} I_{min} &= S.sort[S.sort.index(a) * 0.1\%] \\ I_{max} &= S.sort[-(S.length - S.sort.index(a)) * 0.1\%] \end{aligned} \quad (9)$$

where S is the group of image pixel values for each $R, G \& B$ channel, $S.sort$ is the increasing sorted data set, $S.sort.index(a)$ is the index number of the mode in the histogram

distribution, and $S.sort[x]$ is the value at index x of the positive sorted data set. To implement the unique approach, we extract pixels values in the lowest 0.1% of the left side and the largest 0.1% of the right side from histogram distribution using Eq. (9). The RGB channels and different images of the Rayleigh distribution, the I_{min} and I_{max} are both channel and image sensitive.

Global histogram stretching of $[0, 255]$ range typically results in excessive blue and green light in underwater images. We dynamically decide the highest (O_{max}) and lowest (O_{min}) intensity level values by each RGB channel to obtain a perfect intended band of stretching.

We begin by calculating the Rayleigh distribution's standard deviation values σ_λ , as shown in Eq. (10).

$$\sigma_\lambda = \sqrt{\frac{4 - \pi}{2}} a_\lambda = 0.655 a_\lambda, \lambda \in \{R, G, B\} \quad (10)$$

where a denotes the channel mode, λ belongs to RGB Channels. After that, we establish the required range's minimum value $O_{\lambda min}$, as shown in Eq. (11)

$$O_{\lambda min} = a_\lambda - \beta_\lambda * \sigma_\lambda, 0 \leq O_{\lambda min} \leq I_{\lambda min} \quad (11)$$

Here β_λ is derived from Eq. (11) and substitute σ_λ from Eq. (10)

$$\beta_\lambda = \frac{a_\lambda - O_{\lambda min}}{\sigma_\lambda}, \frac{a_\lambda - I_{min}}{\sigma_\lambda} \leq \beta_\lambda \leq \frac{a_\lambda}{\sigma_\lambda} \quad (12)$$

In the right side of Eq. (12), we get $\beta_\lambda \geq 0$, as $a \geq I_{min}$.

Now, substitute the value of σ_λ in the right side in Eq. (12), we obtain $\beta_\lambda \leq 1.526$.

Now describe $\beta_\lambda \in \mathbb{Z}$, it must have a unique solution that is $\beta_\lambda = 1$. Hence Eq. (11) is rewritten in the form of Eq. (13) as shown below:

$$O_{\lambda min} = a_\lambda - \sigma_\lambda \quad (13)$$

Because of the varying degrees of depletion of the various bands of light in underwater, we should study individual R, G, B channel to compute optimum parameters of the required range. Based on the simple fuzzy image method (1), the image dehazing function $J_\lambda(x)$ is improved as shown in Eq. (14)

$$J_\lambda(x) = \frac{I_\lambda(x) - (1 - t_\lambda(x))B_\lambda}{kt_\lambda(x)} \quad (14)$$

where the red and the green–blue channel have experienced values of 1.1 and 0.9, respectively. When maximizing the recovered image $J_\lambda(x)$, as shown in Eq. (15), the maximum value of the required range O_{max} is obtained.

$$Max(J_\lambda(x)) = Max\left(\frac{I_\lambda(x) - (1 - t_\lambda(x))B_\lambda}{kt_\lambda(x)}\right) \quad (15)$$

B_λ is 0, when $J_\lambda(x)$ reaches its maximum value. Then, for each color channel O_{max} is defined as shown in Eq. (16).

$$O_{\lambda max} = \frac{I_\lambda}{kt_\lambda} = \frac{a_\lambda + \mu_\lambda * \sigma_\lambda}{k * t_\lambda}, I_{\lambda max} \leq O_{\lambda max} \leq 255 \quad (16)$$

$t_\lambda(x)$ is calculated with the help of Eq. (2), where $NRER(\lambda)$ values are 0.83, 0.95 and 0.97 for the RGB channels, respectively (also look at Eq. (3)). Due the estimated path between the camera and the site, $d(x)$ is fixed to 3.

The coefficient μ_λ fulfils the inequality as shown in Eq. (17), depending on the overall range value of $O_{\lambda\max}$.

$$\mu_\lambda = \frac{(O_{\lambda\max} * k * t_\lambda) - a_\lambda}{\sigma_\lambda}$$

$$\frac{k * t_\lambda * I_\lambda}{\sigma_\lambda} \leq \mu_\lambda + 1.526 \leq \frac{k * t_\lambda * 255}{\sigma_\lambda} \quad (17)$$

In Eq. (17), in the integer field μ_λ has either no solution or specific solutions. We take the mean of all solutions when μ_λ are many solutions. When there are no solutions of μ_λ , $O_{\lambda\max}$ is set to 255. These adaptive parameters, which are derived from the histogram distributions from several channels, may substantially enhance the contrast of stretched images while also reducing noise and preserving features.

3.2 Color improvement

Figure 3 shows the sequence used in color improvement.

3.2.1 CIELAB color model

The human eye is capable of seeing large numbers of colors. However, it does not always differentiate between colors properly. Based on our viewing position and illumination, we may see two slightly different colors as the same or detect distinctions in things of equal color. These create challenges when we try to enhance the color component. To enhance the color of underwater images every time, we need strategies to define a color's qualities and identify the quantitative difference between shades. CIELAB, generally CIE $L^*a^*b^*$, is a three dimensional color space that is device independent and enables for exact analysis and measurement of all observable colors via three color variables. In this color space,

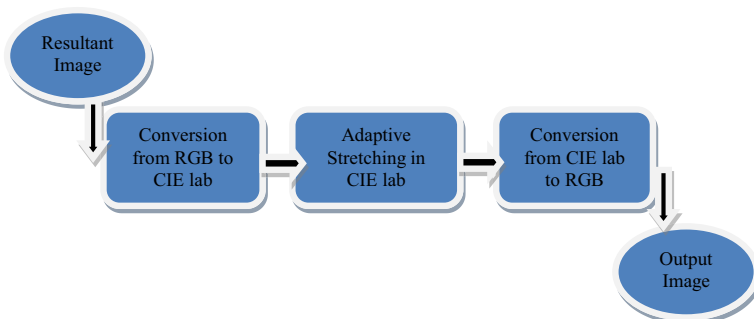


Fig. 3 Sequence used in color improvement

numerical changes between values generally correlate to the degree of difference in colors that humans perceive.

Each of the three variables used by the CIELAB color space to measure objective color and calculate color differences is given by L^* , a^* , and b^* . L^* signifies brightness within a range of 0 to 100. Whereas a^* & b^* signify chromaticity without numerical boundaries. (-ve) a^* represents green, (+ve) a^* represents red, (-ve) b^* represents blue, and (+ve) b^* represents yellow. The CIELAB color space plots a color's location in a chart that comprises an unlimited range of different colors, including colors outside the visible spectrum, by measurements of its L^* , a^* , and b^* values. We may utilize formulas to quantify the difference between distinct colors with the values on the L^* a^* b^* chart, which is referred to as Delta (Δ). To compute L^* , for example, reduce the L^* value of the standard color from the L^* value of the sample. $L^*a^*b^*$ values can also be used to transform to a different color scale. Because of these various qualities of the CIE Lab color model, it is chosen over other models.

3.2.2 Adaptive stretching in CIE lab

Now, resultant image will be color corrected after the contrast enhancement in the RGB color space. To enhance color quality, the image is transformed further into CIELAB color space in this step. The 'L' parameter is similar to image lightness in CIE-Lab color model, provides the darkest assessment at $L=0$ whereas the brightest assessment at $L=100$. The color channel will show true neutral gray values when 'a' and 'b' are both zero. As a result, the output color successions in 'a', 'b' parameters are updated to obtain proper color improvement, while the intensity of the full image is tuned using 'L' component.

The 'L' component is used in conjunction with linear slide stretching, as described in Eq. (8), which lies within 0.1% to 99.9% is stretched to [0 to 100]. The minimum and maximum 0.1% of the image's value is adjusted to 0 & 100, respectively.

'a', 'b' have values ranging [128, 127], where 0 represents the median. An S-model curve is used to define the extending of 'a' and 'b' parameters as shown in Eq. (18).

$$P_\gamma = I_\gamma * \left(\varphi^{1 - \left| \frac{I_\gamma}{128} \right|} \right), \gamma \in \{a, b\} \quad (18)$$

where I_γ is the input pixels, P_γ is the output pixels. γ represents the 'a', 'b' parameters. φ is the ideally suitable value which is 1.3. The stretching coefficient in Eq. (18) is an exponential function, in which case if the value is close to 0, the more it will be stretched.

The importance of contrast and color in an image's clarity and visibility cannot be overstated. As a result, the background and foreground objects in an image are easily distinguished. The channels are assembled and turned into an RGB color model once the stretching process in $L, a \& b$ elements in CIE Lab has been completed. As the observed and viewable final output image, a contrast improved and color improved result can be formed.

4 Result evaluation and analysis

Our designed technique, which includes saturation equalization, sharpness improvement and contrast improvement is quantitatively and qualitatively correlate to other standard enhancement techniques. He [9] utilized image haze reduction with DCP and is taken as

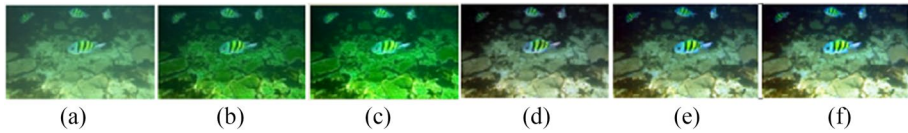


Fig. 4 Represents the (a) Input Image and enhanced images using methods (b) Bianco Prior (c) Dark Channel Prior (d) New Optical Model (e) Unsupervised Color Correction Method (f) Our proposed method

a comparison with our proposed work since it is a traditional approach for dehazing and underwater images are frequently termed haze images. ICM and UCM [23, 25] are the other comparison techniques since they are the most efficient imaging models and have the best similarities to the suggested approach in the context of histogram modification. Because the Rayleigh distribution method failed to run out in [17, 18, 21], we only provide the UCM images in the comparative outcomes because the ICM has comparable outcomes to the UCM. Bianoc Prior (BP) [2] and New Optical Model (NOM) [32] are also compared with our approaches, as they are also based on the single image enhancement system. In our designed technique, as shown in Fig. 4, appears to provide an improved visual image than the other way. UCM and NOM models produces a general sense of fish that has simple changes that do not boost image quality or reduce the brightness and visibility. The BP and DCP oversaturates the color because the image's blue and green colors are dominating in nature, which causes noise and decreases the overall visual effect. As the fisher is more distinguished from the background, the color saturation and the contrast of the image created by our approach improves, and a smaller amount blue green lighting is preserved.

The x-axis in the histogram in input as well as in output images lies from 0 to 255 as shown in the other part of Fig. 5. In (a) and (b) part the gray level values of histogram distributions are relatively dense, which helps to explain why two vibrant pictures have poor contrast and visibility. The gray level values in (c) & (d) spread as comparison to (a) & (b) but not as good with respect to (e) & (f) The gray level values of histogram distribution in (e) & (f) are dispersed

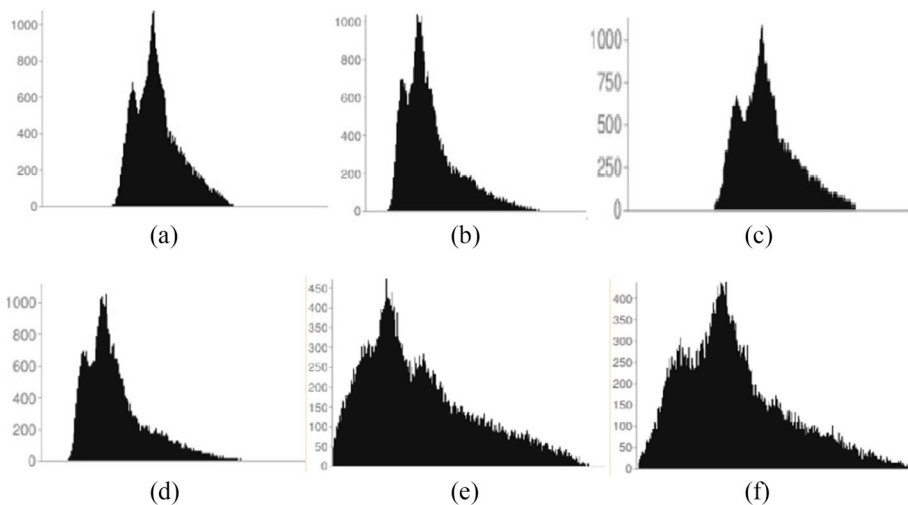


Fig. 5 Represents the histogram distribution of (a) Input Image (b) Bianco Prior (c) Dark Channel Prior (d) New Optical Model (e) Unsupervised Color Correction Method (f) Our proposed method

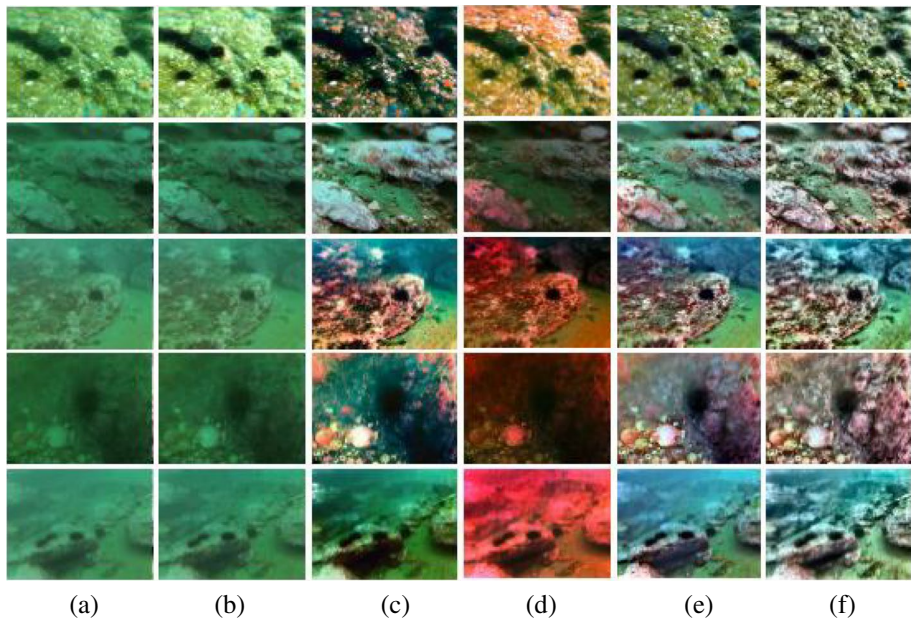


Fig. 6 (a) Input Image (b) Bianco Prior (c) Dark Channel Prior (d) New Optical Model (e) Unsupervised Color Correction Method (f) Our proposed method

throughout the x-axis, but according to GWAT [33], because of the accurate histogram stretching, the histogram of the improved image as shown in (f) has a better distribution.

Various approaches used for image improvement attains the outcome as giving in Fig. 6. Input images are from the Real World Underwater Image Enhancement (RUIE) Data Set. Clearly, the images are not enhanced by BP and NOM as shown in Fig. 6 (b) & Fig. 6 (d). In Fig. 6 (c) & Fig. 6 (e), the top two images of the DCP and UCM oversaturates image color when image's blue & green color gets too intense, resulting in enhanced images that are less realistic than those produced by our technique as shown in Fig. 6 (d) (top two images). The UCM's output underwater images have considerable noise; however our technique successfully reduces the noise while preserving image features as represented in the below three images in Fig. 6 (e) and Fig. 6 (f), respectively.

We use objective metrics like entropy, mean square error (MSE), peak signal to noise ratio (PSNR) [16], High-Dynamic Range Visual Difference Predictor2 (HDR-VDP2) [15] and underwater color image quality evaluation (UCIQE) [36] to perform quantitative analysis. The amount of information is represented by entropy, which is understood as the mean unpredictability of the information source. The more information there is, the greater the entropy value. MSE and PSNR are standard image quality evaluation measures that primarily measure image noise deterioration. The HDR-VDP2 predicts both the presence of artefacts and the overall quality of images using a pretty complex model of human perception. It generates a QMOS value ranging from 0 (best) to 100 (worst) to represent image quality. The UCIQE, which is an appropriate analytical predictor of hue, brightness, and contrast, is a relatively new non reference metrics for the evaluation of color image quality. However, MSE, PSNR and Q-MOS are full reference metrics that take an actual image as a reference. They can be used to show how the created image compares to the original in terms of observed loss in quality and increase in noise. The comparative outcomes with following evaluation models

are given in Table 1. We compared our Comparative Universal Stretching model with Bianco Prior [32], Dark Channel Prior [9], New Optical Model [33], Integrated Color Model [23], and Unsupervised Color Correction Method [25]. In the assessments, our method comparative universal stretching gets the highest outcomes while in Unsupervised Color Correction gets the second highest outcomes. The Bianco Prior and Dark Channel Prior methods are based on the underwater image restoration method. The New Optical and Integrated Color Models are based on the underwater image enhancement method. The Comparative Universal stretching is also uses fusion based approach in underwater image enhancement method.

It keeps the most details and information, provides excellent visibility, overall quality and reduces noise. The greatest UCIQE score indicates that our approach can properly balance the improved underwater images' chroma, saturation, and contrast. In all four approaches, the DCP delivers the lowest results, which is constant with the viewing experience of low brightness and poor visibility. This implies that basic haze elimination with the DCP to underwater enhancement should not be employed straight forward. The UCM and ICM technique generate images having visible noise, resulting in a high MSE and low PSNR value.

Figure 7 represents the underwater images and their corresponding enhanced images from eight different datasets having Underwater Test Dataset (U45) [5] in Fig. 7(a), Enhancing Underwater Visual Perception (EUVP) [14] in Fig. 7(b), Underwater Image Enhanced Benchmark dataset (UIEB) [26] in Fig. 7(c), Large-scale Underwater Image (LSUI) dataset [38] in Fig. 7(d), UFO-120 dataset [6] in Fig. 7(e), Real-world Underwater Image Enhancement (RUIE) dataset [39] in Fig. 7(f), Underwater MOT dataset [19] in Fig. 7(g) and dataset for Underwater object detection (DUO) [22] in Fig. 7(h). The size of the input images is of $1360 * 1024$. Table 2, represents the evaluation metrics in the form of MSE, PSNR, UCIQE and UIQM values of four enhanced images of each eight datasets which have been shown in Fig. 7.

Tables 3, 4, 5, 6, 7, 8, 9 and Table 10 represents the quantitative analysis of all eight datasets in detail. In each table, ten random test sample images have been chosen to compute evaluation metrics. In these tables, the bold values given in RMSE, PSNR, UCIQE, and UIQM represent the average values of the sample images for each dataset. The chosen images are totally different from all the above images, which have been used in Fig. 7. On the basis of the RMSE evaluation parameter, the top two results have been seen in the UIEB dataset, i.e., 731.326, and the RUIE dataset, i.e., 818.134, whereas the bottom two results have been seen in the LSUI dataset, i.e., 1093.794, and the Underwater MOT dataset, i.e., 1232.432. With the PSNR evaluation parameter, the top two results have been seen in the UIEB dataset, i.e., 18.366, and the EUVP dataset, i.e., 17.353, whereas the bottom two results have been seen in the LSUI dataset, i.e., 15.878, and the DUO dataset, i.e., 16.493. With the UCIQE evaluation parameter, the top two results have been seen in the UIEB dataset, i.e., 0.513, and the RUIE dataset, i.e., 0.486, whereas the bottom two results have been seen in the LSUI dataset, i.e.,

Table 1 Evaluation of various methods based on entropy, MSE, PSNR, HDR-VDP2 and UCIQE

Methods	ENTROPY	MSE	PSNR	HDR-VDP2	UCIQE	UIQM
Bianco Prior [32]	5.432	3201.665	12.641	55.896	0.401	0.114
Dark Channel Prior [9]	6.172	3116.789	13.361	53.688	0.419	1.396
New Optical Model [33]	6.554	2224.367	15.512	48.369	0.453	1.327
Integrated Color Model [23]	7.224	1440.126	16.582	42.657	0.485	2.236
Unsupervised Color Correction Method [25]	7.567	1355.568	16.973	38.666	0.528	2.668
Comparative Universal Stretching	7.887	920.205	18.924	33.695	0.596	2.734

Table 2 Evaluation Metrics of our proposed method on various datasets using MSE, PSNR, UCIQE and UIQM

Dataset	Images	RMSE	PSNR	UCIQE	UIQM
U45	Figure 7 (a) (i)	1389.985	17.369	0.489	2.123
	Figure 7 (a) (ii)	1458.398	16.254	0.456	1.965
	Figure 7 (a) (iii)	1187.325	17.321	0.496	1.587
	Figure 7 (a) (iv)	1255.985	15.323	0.532	2.321
EUVP	Figure 7 (b) (i)	1026.987	16.548	0.498	2.541
	Figure 7 (b) (ii)	826.698	17.896	0.562	2.365
	Figure 7 (b) (iii)	855.258	17.549	0.554	2.897
	Figure 7 (b) (iv)	812.987	18.369	0.589	3.168
UIEB	Figure 7 (c) (i)	750.357	19.398	0.599	3.245
	Figure 7 (c) (ii)	712.987	19.687	0.601	3.112
	Figure 7 (c) (iii)	650.325	18.368	0.532	2.987
	Figure 7 (c) (iv)	623.245	19.967	0.491	2.645
LSUI	Figure 7 (d) (i)	1055.325	15.359	0.402	1.987
	Figure 7 (d) (ii)	1032.357	16.356	0.425	2.665
	Figure 7 (d) (iii)	1652.365	16.245	0.489	1.986
	Figure 7 (d) (iv)	984.325	17.554	0.487	1.889
UFO-120	Figure 7 (e) (i)	820.125	15.748	0.523	2.568
	Figure 7 (e) (ii)	850.256	15.356	0.432	2.325
	Figure 7 (e) (iii)	1052.658	16.958	0.489	2.578
	Figure 7 (e) (iv)	981.854	17.698	0.502	2.222
RUIE	Figure 7 (f) (i)	752.995	19.689	0.569	3.568
	Figure 7 (f) (ii)	715.658	19.584	0.635	3.115
	Figure 7 (f) (iii)	655.358	19.284	0.555	2.998
	Figure 7 (f) (iv)	620.356	19.657	0.489	2.897
Underwater MOT	Figure 7 (g) (i)	1110.879	16.358	0.502	3.589
	Figure 7 (g) (ii)	1204.689	16.325	0.565	3.456
	Figure 7 (g) (iii)	1002.359	18.658	0.486	2.154
	Figure 7 (g) (iv)	995.987	17.658	0.466	2.753
DUO	Figure 7 (h) (i)	1056.337	16.526	0.416	3.129
	Figure 7 (h) (ii)	985.401	15.469	0.337	2.101
	Figure 7 (h) (iii)	1054.159	16.334	0.499	3.825
	Figure 7 (h) (iv)	9987.232	17.567	0.562	2.219

0.415, and the Underwater MOT dataset, i.e., 0.398. With the UIQM evaluation parameter, the top two results have been seen in the RUIE dataset, i.e., 2.750, and the UFO-120 dataset, i.e., 2.632, whereas the bottom two results have been seen in the LSUI dataset, i.e., 2.420, and the Underwater MOT dataset, i.e., 1.935.

If the RMSE value is lower, then the image quality is better, whereas if the PSNR, UCIQE, and UIQM values are higher, the image is better. If the average value of any dataset in the test samples is less than 1000 in RMSE and greater than 16.700, 0.450, and 2.500 in PSNR, UCIQE, and UIQM, respectively, we consider our method to be above average for the datasets; otherwise, we consider our method to be below average for the datasets. Using these qualitative and quantitative analyses, we can easily conclude that the images enhanced using our comparative universal stretching method in the UIEB, RUIE, EUVP, UFO-120, and U45 datasets are above average, while those in

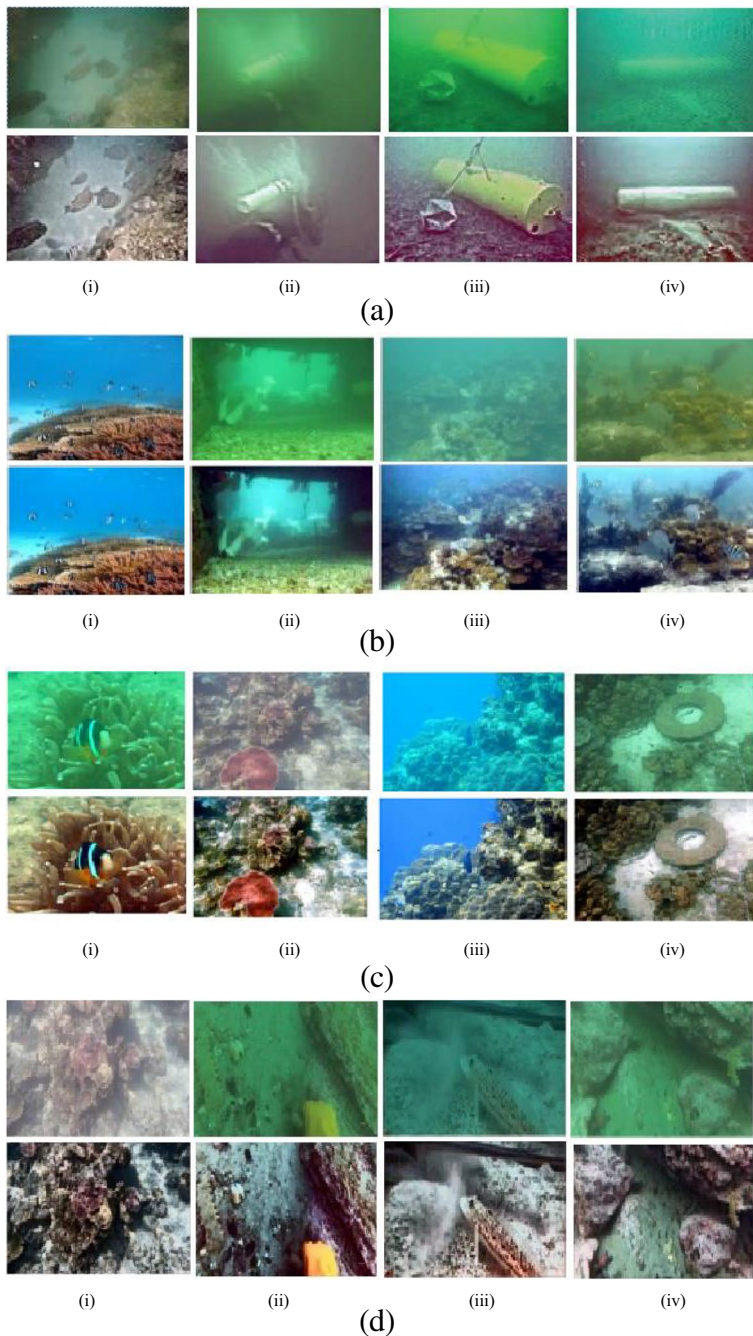


Fig. 7 (a) U45 datasets input and enhanced images (b) EUVP datasets input and enhanced images (c) UIEB datasets input and enhanced images (d) LSUI datasets input and enhanced images (e) UFO-120 datasets input and enhanced images (f) RUIE datasets input and enhanced images (g) Underwater MOT datasets input and enhanced images (h) DUO datasets input and enhanced images.

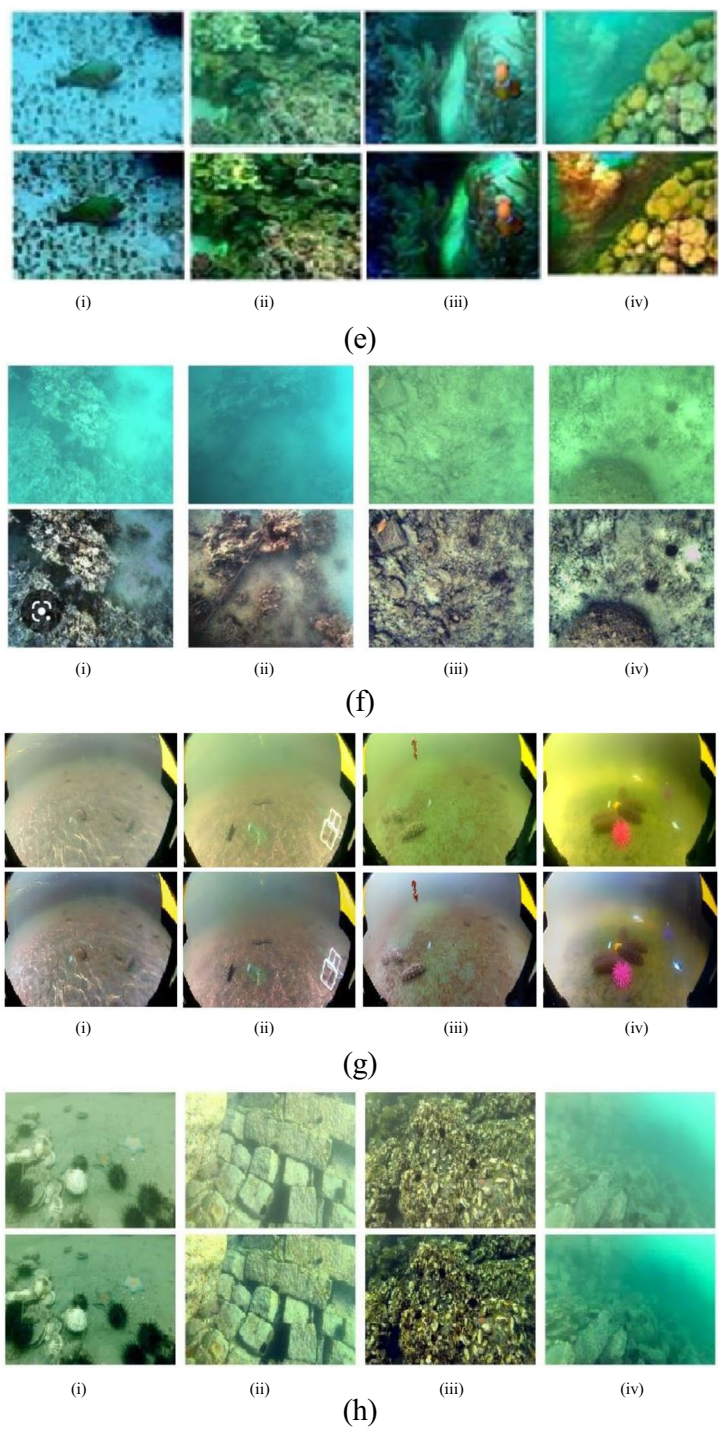


Fig. 7 (continued)

Table 3 Evaluation Metrics of our proposed method on U45 dataset using MSE, PSNR, UCIQE and UIQM

Dataset	Images	RMSE	PSNR	UCIQE	UIQM
U45	Sample Image 1	1040.709	17.441	0.436	2.302
	Sample Image 2	905.390	17.435	0.441	3.589
	Sample Image 3	989.783	17.000	0.478	1.666
	Sample Image 4	822.131	16.255	0.423	1.863
	Sample Image 5	1071.325	16.235	0.456	2.365
	Sample Image 6	1074.658	17.321	0.569	3.265
	Sample Image 7	1018.698	17.256	0.444	1.325
	Sample Image 8	979.258	17.369	0.565	2.325
	Sample Image 9	1085.147	16.357	0.462	2.654
	Sample Image 10	906.963	17.238	0.423	3.698
	Sample Image Average	989.406	16.991	0.470	2.505

Table 4 Evaluation Metrics of our proposed method on EUVP dataset using MSE, PSNR, UCIQE and UIQM

Dataset	Images	RMSE	PSNR	UCIQE	UIQM
EUVP	Sample Image 1	842.026	15.749	0.419	1.864
	Sample Image 2	872.154	17.275	0.418	2.137
	Sample Image 3	830.644	15.534	0.430	1.661
	Sample Image 4	872.253	15.822	0.422	2.247
	Sample Image 5	1022.762	17.987	0.445	2.156
	Sample Image 6	922.121	18.654	0.556	3.654
	Sample Image 7	913.356	18.123	0.456	2.355
	Sample Image 8	1184.800	18.357	0.564	2.658
	Sample Image 9	1045.131	18.456	0.598	3.325
	Sample Image 10	1134.175	17.569	0.444	2.298
	Sample Image Average	963.942	17.353	0.475	2.436

Table 5 Evaluation Metrics of our proposed method on UIEB dataset using MSE, PSNR, UCIQE and UIQM

Dataset	Images	RMSE	PSNR	UCIQE	UIQM
UIEB	Sample Image 1	606.608	16.095	0.465	1.887
	Sample Image 2	662.074	17.776	0.459	2.107
	Sample Image 3	767.527	16.592	0.401	1.888
	Sample Image 4	727.181	17.663	0.410	1.904
	Sample Image 5	798.359	18.862	0.625	2.632
	Sample Image 6	780.157	18.426	0.588	2.231
	Sample Image 7	759.153	19.842	0.564	3.214
	Sample Image 8	684.953	19.874	0.489	3.278
	Sample Image 9	763.759	18.896	0.525	3.865
	Sample Image 10	763.486	19.632	0.608	2.536
	Sample Image Average	731.326	18.366	0.513	2.554

Table 6 Evaluation Metrics of our proposed method on LSUI dataset using MSE, PSNR, UCIQE and UIQM

Dataset	Images	RMSE	PSNR	UCIQE	UIQM
LSUI	Sample Image 1	1043.574	15.366	0.441	1.827
	Sample Image 2	1020.682	15.576	0.405	2.333
	Sample Image 3	1252.697	15.006	0.467	1.921
	Sample Image 4	979.576	16.699	0.439	1.790
	Sample Image 5	1163.800	16.933	0.307	2.787
	Sample Image 6	1255.143	17.116	0.369	2.636
	Sample Image 7	908.869	15.056	0.309	2.462
	Sample Image 8	1006.861	15.025	0.476	2.095
	Sample Image 9	1241.307	16.407	0.471	3.168
	Sample Image 10	915.795	15.664	0.404	3.221
	Sample Image Average	1093.794	15.878	0.415	2.420

Table 7 Evaluation Metrics of our proposed method on UFO-120 dataset using MSE, PSNR, UCIQE and UIQM

Dataset	Images	RMSE	PSNR	UCIQE	UIQM
UFO-120	Sample Image 1	820.711	16.779	0.414	1.613
	Sample Image 2	818.224	16.771	0.496	1.737
	Sample Image 3	816.678	15.337	0.500	2.449
	Sample Image 4	847.085	15.109	0.427	2.058
	Sample Image 5	1060.826	17.567	0.472	2.905
	Sample Image 6	976.274	17.779	0.487	2.202
	Sample Image 7	1113.448	16.119	0.452	3.934
	Sample Image 8	1150.686	18.752	0.420	3.876
	Sample Image 9	1169.523	15.155	0.467	3.182
	Sample Image 10	1128.895	15.343	0.428	2.584
	Sample Image Average	991.216	16.584	0.454	2.623

Table 8 Evaluation Metrics of our proposed method on RUIE dataset using MSE, PSNR, UCIQE and UIQM

Dataset	Images	RMSE	PSNR	UCIQE	UIQM
RUIE	Sample Image 1	706.448	15.604	0.446	1.755
	Sample Image 2	663.923	17.641	0.410	2.306
	Sample Image 3	697.657	16.949	0.500	2.194
	Sample Image 4	705.228	15.570	0.414	2.064
	Sample Image 5	979.839	17.907	0.423	3.228
	Sample Image 6	864.686	18.933	0.579	2.655
	Sample Image 7	997.312	16.036	0.503	3.550
	Sample Image 8	833.470	17.422	0.493	3.846
	Sample Image 9	914.562	17.945	0.502	3.725
	Sample Image 10	818.213	17.041	0.586	2.180
	Sample Image Average	818.134	17.105	0.486	2.750

Table 9 Evaluation Metrics of our proposed method on Underwater MOT dataset using MSE, PSNR, UCIQE and UIQM

Dataset	Images	RMSE	PSNR	UCIQE	UIQM
Underwater MOT	Sample Image 1	1099.793	15.898	0.490	1.987
	Sample Image 2	1253.287	15.166	0.464	1.601
	Sample Image 3	1033.680	17.286	0.405	1.543
	Sample Image 4	1129.493	17.313	0.415	2.484
	Sample Image 5	1287.365	17.687	0.352	1.957
	Sample Image 6	1343.265	15.572	0.342	1.938
	Sample Image 7	1338.458	15.521	0.380	1.929
	Sample Image 8	1254.369	17.355	0.435	2.018
	Sample Image 9	1303.245	18.895	0.375	2.058
	Sample Image 10	1281.365	17.529	0.323	1.837
	Sample Image Average	1232.432	16.822	0.398	1.935

the LSUI, Underwater MOT, and DUO datasets are below average. Hence, the overall results of our proposed method are better in these datasets compared to other methods.

To prove the robustness of our approach, we took input images from different datasets and then performed our technique to improve the underwater images. In most of the datasets, our designed technique gives the best results, whereas in some datasets the results are below average. But the overall performance of our approach is above average. To summaries, the research suggests that our technique is better to commonly used underwater image enhancement methods in producing high-quality underwater images.

5 Conclusion and discussion

In this research, we analyzed challenges with water images and videos and current underwater image improvement methods, and successfully suggested a novel image enhancement approach called CUS for a variety of underwater images. Various underwater image enhancement algorithms and methods have been used to improve the

Table 10 Evaluation Metrics of our proposed method on DUO dataset using MSE, PSNR, UCIQE and UIQM

Dataset	Images	RMSE	PSNR	UCIQE	UIQM
DUO	Sample Image 1	1045.142	16.548	0.401	3.287
	Sample Image 2	1037.716	16.674	0.441	2.129
	Sample Image 3	960.472	15.987	0.353	2.019
	Sample Image 4	1013.565	16.542	0.441	3.187
	Sample Image 5	924.647	17.341	0.493	2.070
	Sample Image 6	1074.894	16.993	0.437	3.182
	Sample Image 7	813.642	17.086	0.412	2.183
	Sample Image 8	1069.631	16.224	0.338	2.087
	Sample Image 9	969.763	15.074	0.493	2.999
	Sample Image 10	1047.834	16.461	0.431	2.529
	Sample Image Average	995.731	16.493	0.424	2.567

images but they are mostly dataset-specific. We worked not only on the color component but also on the contrast component. This fusion-based enhancement approach is a single image-based system which not only improves the result over other standard methods but also works well on various datasets that's why it is also dataset independent. This dataset-independent approach provides robustness to our model which makes it superior in comparison to other methods. Our suggested model initially conducts contrast improvement using a basic histogram stretching with adaptive characteristics obtained in the RGB color space that considers both the raw image's histogram distribution parameter and underwater propagation capabilities of distinct light channels. The CIE Lab color model is then used to perform adaptive stretching for color improvement. After that our proposed technique is compared to other standard dehazing model DCP, as well as other enhancement models like UCM and ICM. These enhancement models also use histogram stretching in HSI/HSV and R-G-B color space. Qualitative and quantitative findings show that our technique is more successful at increasing visibility, improving details, and reducing artefacts and noise from images. Other underwater image datasets can also benefit from the incorporation of histogram restructuring in RGB and CIE Lab color models. Hence, it shows that our system is highly robust in nature, which provides a fruitful output for different datasets.

In addition, our system enhances the visibility of blurry and low light images. Even though our method outperforms the competition, it has some shortcomings. On one side, our method may have over enhanced regions for underwater images taken in artificial light. While on other side, the process of choosing the CIE lab color space may increase the algorithm's complexity. As a result, we will investigate and solve these issues in future work. The following aspects should also be considered in future research.

- 1) Developing underwater image enhancement systems that is more robust and computationally efficient. The proposed image enhancement approach should be capable of adapting to various underwater environments and developing an effective enhancement strategy for various types of underwater applications. We may conclude from this research that only a few of the techniques can increase the quality of all underwater images.
- 2) Creating a suitable underwater image dataset. There are currently no publicly accessible underwater image datasets, such as pairings of hazed and clear images, background lights of underwater images, depth maps, transmission maps, etc.
- 3) Providing a relationship between low level image processing and high level classification & detection. Existing underwater image enhancement approaches concentrate on increasing image intuitive effects while ignoring whether the improved images may improve the precision of high level characteristics analysis like target recognition and classification.
- 4) Designing an efficient underwater image quality evaluation measure. Although several image quality evaluation measures have been published, only a few in numbers are applicable to underwater images. Here, the commonly used UIQM and UCIQE, which is motivated by human vision structure properties to evaluate underwater color images, failed to give a valid evaluation of quality of underwater image. Their assessment prefers overly-enhanced colored images, which contradicts subjective preferences for naturalness. Future work must be given to the sensible combination of both objective and subjective evaluation, as well as the continuous improvement of non-reference evaluation models.

Funding Any agency does not fund this study.

Data availability The manuscript does not have any associated data which was generated.

Declarations

Conflict of interest All the authors of this paper declare that he/she has no conflict of interest.

Ethical approval This article does not contain any studies with human participants or animals performed by any of the authors.

References


1. Bhat A, Tyagi A, Verdhan A, Verma V (2021) Fast Under Water Image Enhancement for Real Time Applications. In 2021 6th International Conference for Convergence in Technology (I2CT) 1–8
2. Carlevaris-Bianco N, Mohan A, Eustice RM (2010) Initial results in underwater single image dehazing. In Oceans 2010 Mts/IEEE Seattle 1–8
3. Chen BH, Tseng YS, Yin JL (2020) Gaussian-adaptive bilateral filter. *IEEE Signal Process Lett* 27:1670–1674
4. Daway HG, Daway EG (2019) Underwater image enhancement using colour restoration based on YCbCr colour model. In IOP Conference Series: Materials Science and Engineering 571(1):012125
5. Drews PL, Nascimento ER, Botelho SS, Campos MFM (2016) Underwater depth estimation and image restoration based on single images. *IEEE Comput Graphics Appl* 36(2):24–35
6. Fu X, Fan Z, Ling M, Huang Y, Ding X (2017) Two-step approach for single underwater image enhancement. In: 2017 International Symposium on Intelligent Signal Processing and Communication Systems (ISPACS) 789–94
7. Fu Z, Fu X, Huang Y, Ding X (2022) Twice mixing: a rank learning based quality assessment approach for underwater image enhancement. *Signal Processing: Image Communication* 102:116622
8. Galdran A, Pardo D, Picón A, Alvarez-Gila A (2015) Automatic red-channel underwater image restoration. *J Vis Commun Image Represent* 26:132–145
9. Ghani ASA, Isa NAM (2014) Underwater image quality enhancement through Rayleigh-stretching and averaging image planes. *International Journal of Naval Architecture and Ocean Engineering* 6(4):840–866
10. Ghani ASA, Isa NAM (2015) Underwater image quality enhancement through integrated color model with Rayleigh distribution. *Appl Soft Comput* 27:219–230
11. Ghani ASA, Isa NAM (2015) Enhancement of low quality underwater image through integrated global and local contrast correction. *Appl Soft Comput* 37:332–344
12. Ghani ASA, Aris RSNAR, Zain MLM (2016) Unsupervised contrast correction for underwater image quality enhancement through integrated-intensity stretched-Rayleigh histograms. *Journal of Telecommunication Electronic and Computer Engineering (JTEC)* 8(3):1–7
13. Gupta S, Mohan N, Kumar M (2021) A study on source device attribution using still images. *Archives of Computational Methods in Engineering* 28(4):2209–2223
14. Han R, Guan Y, Yu Z, Liu P, Zheng H (2020) Underwater Image Enhancement Based on a Spiral Generative Adversarial Framework. *IEEE Access* 8:218838–218852
15. He K, Sun J, Tang X (2010) Single image haze removal using dark channel prior. *IEEE Trans Pattern Anal Mach Intell* 33(12):2341–2353
16. Iqbal K, Odetayo M, James A, Salam RA, Talib AZH (2010) Enhancing the low quality images using Unsupervised Color Improvement Method. In IEEE International Conference on Systems, Man and Cybernetics 1703–1709
17. Islam MJ, Luo P, Sattar J (2020) Simultaneous enhancement and super-resolution of underwater imagery for improved visual perception. *arXiv preprint arXiv:2002.01155*
18. Islam MJ, Xia Y, Sattar J (2020) Fast underwater image enhancement for improved visual perception. *IEEE Robotics and Automation Letters* 5(2):3227–3234
19. Lai Y, Zhou Z, Su B, Xuanyuan Z (2022) Single underwater image enhancement based on differential attenuation compensation. *Frontiers in Marine Science* 2216
20. Lee Z, Shang S, Hu C, Du K, Weidemann A, Hou W, Lin J, Lin G (2015) Secchi disk depth: A new theory and mechanistic model for underwater visibility. *Remote Sens Environ* 169:139–149
21. Li CY, Guo JC, Cong RM, Pang YW, Wang B (2016) Underwater image enhancement by dehazing with minimum information loss and histogram distribution prior. *IEEE Trans Image Process* 25(12):5664–5677

22. Li Y, Lu H, Li J, Li X, Li Y, Serikawa S (2016) Underwater image de-scattering and classification by deep neural network. *Comput Electr Eng* 54:68–77
23. Li C, Guo J, Guo C (2018) Emerging from water: Underwater image color correction based on weakly supervised color transfer. *IEEE Signal Process Lett* 25(3):323–327
24. Li C, Guo C, Ren W, Cong R, Hou J, Kwong S, Tao D (2019) An underwater image enhancement benchmark dataset and beyond. *IEEE Trans Image Process* 29:4376–4389
25. Liu C, Li H, Wang S, Zhu M, Wang D, Fan X, Wang Z (2021) A dataset and benchmark of underwater object detection for robot picking. *IEEE International Conference on Multimedia & Expo Workshops (ICMEW)* 1–6
26. Liu R, Fan X, Zhu M, Hou M, Luo Z (2020) Real-world underwater enhancement: Challenges, benchmarks, and solutions under natural light. *IEEE Trans Circuits Syst Video Technol* 30(12):4861–4875
27. Middleton WEK (1957) Vision through the atmosphere. In *geophysik ii/geophysics ii* Springer, Berlin, Heidelberg, pp 254–287
28. Narvaria M, Mantiuk R, Da Silva MP, Le Callet P (2015) HDR-VDP-2.2: a calibrated method for objective quality prediction of high-dynamic range and standard images. *Journal of Electronic Imaging* 24(1):010501
29. Peng L, Zhu C, Bian L (2021) U-shape Transformer for Underwater Image Enhancement. *arXiv pre-print arXiv:2111.11843*
30. Schettini R, Corchs S (2010) Underwater image processing: state of the art of restoration and image enhancement methods. *EURASIP Journal on Advances in Signal Processing* 1–14
31. Shen L, Zhao Y, Peng Q, Chan JCW, Kong SG (2018) An iterative image dehazing method with polarization. *IEEE Trans Multimedia* 21(5):1093–1107
32. Singh N, Bhat A (2021) A Detailed Understanding of Underwater Image Enhancement using Deep Learning. In *5th International Conference on Information Systems and Computer Networks (ISCON)* 1–6
33. Soni OK, Kumare JS (2020) A survey on underwater images enhancement techniques. In *IEEE 9th International Conference on Communication Systems and Network Technologies (CSNT)* 333–338
34. Tamou AB, Benzinou A, Nasreddine K, Ballihi L (2018) Underwater live fish recognition by deep learning. In *International Conference on Image and Signal Processing*, Springer, Cham 275–283
35. Ulutas G, Ustubioglu B (2021) Underwater image enhancement using contrast limited adaptive histogram equalization and layered difference representation. *Multimedia Tools and Applications* 80(10):15067–15091
36. Wen H, Tian Y, Huang T, Gao W (2013) Single underwater image enhancement with a new optical model. In *2013 IEEE International Symposium on Circuits and Systems (ISCAS)* 753–756
37. Yang M, Sowmya A (2015) An underwater color image quality evaluation metric. *IEEE Trans Image Process* 24(12):6062–6071
38. Zhang W, Pan X, Xie X, Li L, Wang Z, Han C (2021) Color correction and adaptive contrast enhancement for underwater image enhancement. *Comput Electr Eng* 91:106981
39. Zhao X, Jin T, Qu S (2015) Deriving inherent optical properties from background color and underwater image enhancement. *Ocean Eng* 94:163–172

Publisher's note Springer Nature remains neutral with regard to jurisdictional claims in published maps and institutional affiliations.

Springer Nature or its licensor (e.g. a society or other partner) holds exclusive rights to this article under a publishing agreement with the author(s) or other rightsholder(s); author self-archiving of the accepted manuscript version of this article is solely governed by the terms of such publishing agreement and applicable law.

Authors and Affiliations

Nishant Singh¹ · Aruna Bhat² 

¹ Department of Computer Science & Engineering, Delhi Technological University, Delhi 110042, Delhi, India

² Department of Computer Science & Engineering, Delhi Technological University, Delhi 110042, Delhi, India

Terms and Conditions

Springer Nature journal content, brought to you courtesy of Springer Nature Customer Service Center GmbH (“Springer Nature”).

Springer Nature supports a reasonable amount of sharing of research papers by authors, subscribers and authorised users (“Users”), for small-scale personal, non-commercial use provided that all copyright, trade and service marks and other proprietary notices are maintained. By accessing, sharing, receiving or otherwise using the Springer Nature journal content you agree to these terms of use (“Terms”). For these purposes, Springer Nature considers academic use (by researchers and students) to be non-commercial.

These Terms are supplementary and will apply in addition to any applicable website terms and conditions, a relevant site licence or a personal subscription. These Terms will prevail over any conflict or ambiguity with regards to the relevant terms, a site licence or a personal subscription (to the extent of the conflict or ambiguity only). For Creative Commons-licensed articles, the terms of the Creative Commons license used will apply.

We collect and use personal data to provide access to the Springer Nature journal content. We may also use these personal data internally within ResearchGate and Springer Nature and as agreed share it, in an anonymised way, for purposes of tracking, analysis and reporting. We will not otherwise disclose your personal data outside the ResearchGate or the Springer Nature group of companies unless we have your permission as detailed in the Privacy Policy.

While Users may use the Springer Nature journal content for small scale, personal non-commercial use, it is important to note that Users may not:

1. use such content for the purpose of providing other users with access on a regular or large scale basis or as a means to circumvent access control;
2. use such content where to do so would be considered a criminal or statutory offence in any jurisdiction, or gives rise to civil liability, or is otherwise unlawful;
3. falsely or misleadingly imply or suggest endorsement, approval, sponsorship, or association unless explicitly agreed to by Springer Nature in writing;
4. use bots or other automated methods to access the content or redirect messages
5. override any security feature or exclusionary protocol; or
6. share the content in order to create substitute for Springer Nature products or services or a systematic database of Springer Nature journal content.

In line with the restriction against commercial use, Springer Nature does not permit the creation of a product or service that creates revenue, royalties, rent or income from our content or its inclusion as part of a paid for service or for other commercial gain. Springer Nature journal content cannot be used for inter-library loans and librarians may not upload Springer Nature journal content on a large scale into their, or any other, institutional repository.

These terms of use are reviewed regularly and may be amended at any time. Springer Nature is not obligated to publish any information or content on this website and may remove it or features or functionality at our sole discretion, at any time with or without notice. Springer Nature may revoke this licence to you at any time and remove access to any copies of the Springer Nature journal content which have been saved.

To the fullest extent permitted by law, Springer Nature makes no warranties, representations or guarantees to Users, either express or implied with respect to the Springer nature journal content and all parties disclaim and waive any implied warranties or warranties imposed by law, including merchantability or fitness for any particular purpose.

Please note that these rights do not automatically extend to content, data or other material published by Springer Nature that may be licensed from third parties.

If you would like to use or distribute our Springer Nature journal content to a wider audience or on a regular basis or in any other manner not expressly permitted by these Terms, please contact Springer Nature at

onlineservice@springernature.com